Sensors and Materials, Vol. 35, No. 5 (2023) 1599–1612
MYU Tokyo

S & M 3273

Novel Portable 2.4 GHz Antenna Beam Sensor

Ja-Hao Chen,[1*] Yu-Chang Lin,[2] Tai-Chieh Tseng,[1] and Cheng-Chi Yu[1]

[1]Department of Communication Engineering, Feng Chia University,
No. 100, Wenhwa Rd., Seatwen, Taichung 407102, Taiwan (R.O.C.)
[2]Ph.D. Program of Electrical and Communications Engineering, Feng Chia University,
No. 100, Wenhwa Rd., Seatwen, Taichung 407102, Taiwan (R.O.C.)

(Received August 5, 2022; accepted March 28, 2023)

Keywords: antenna beam sensor, RF rectenna, wireless power transmission system, radio frequency energy harvesting

A novel portable 2.4 GHz antenna beam sensor has been designed and implemented. The functions of the proposed sensor are to observe the spatial radiation distribution by using vision and to measure the spatial radiation power intensity distribution. The antenna beam sensor comprises a 6 × 6 radio frequency (RF) rectenna array. Each RF rectenna is a combination of a patch antenna and a high-efficiency radio frequency–direct current (RF–DC) conversion circuit. The output of each RF rectenna is connected to an LED, and the location of the spatial beam power intensity is determined from the luminous intensity of the LED. Additionally, the spatial beam power intensity distribution is obtained by measuring the output voltage of the RF rectennas. The patch antenna size is 7 × 7 cm^2, the measured reflection coefficient of the antenna is greater than 10 dB at 2.4 GHz, and the measured antenna maximum gain is 5.1 dBi. The RF–DC conversion circuit is designed with a 2.4 GHz ten-stage Cockcroft–Walton voltage multiplier rectifier circuit, which can improve the conversion efficiency and beam sensing sensitivity. The RF–DC conversion circuit size is 3.5 × 4.7 cm^2. The measured reflection coefficient of the circuit is greater than 10 dB at 2.4 GHz, and the highest measured conversion efficiency is 50.38%. The overall size of the antenna beam sensor is 42 × 42 cm^2 and the weight is 1.15 kg. Therefore, the sensor is light and easy to handle, which makes it easy to carry for measurement work. This proposed antenna beam sensor is useful for applications in the research of wireless power transfer, microwave energy harvesting, and antenna radiation beam behavior in air.

1. Introduction

The global Internet of Things (IoT) technology is developing rapidly, and a large number of sensing devices have been installed over the past five years. According to the forecast from the Transform Insights TAM Forecast Database, there will be 24.1 billion active IoT devices in 2030.(1) Thus, powering this tremendous number of IoT devices will become a great challenge. Conventional ways of powering devices, such as connecting

*Corresponding author: e-mail: chiahaoc@fcu.edu.tw
https://doi.org/10.18494/SAM4076

ISSN 0914-4935
https://myukk.org/

power cords or using batteries that must be regularly replaced, require huge amounts of resources not only to support the setup cost and maintenance work but also to maintain the quality of service when it comes to large-scale IoT connectivity. Then, to resolve the power supply issue, it is obvious that IoT devices that communicate wirelessly will become most effective with the application of a wireless power supply.

Over several decades, various wireless charger technologies have been published. Near-field wireless power transfer (WPT) based on inductive power transfer has been realized with commercial products that can charge mobile devices.(2) However, despite the high-efficiency charge performance of near-field WPT, it is extremely limited for IoT applications owing to its short charging range. To achieve long-distance wireless power transfer, radio frequency (RF) WPT technology is the most commonly considered method. It is reported that RF WPT technology can be used to wirelessly transmit power to IoT devices up to hundreds of meters away.(3) However, the primary obstacle to RF WPT is the low power transfer efficiency since most of the natural dispersive RF power dissipates in air. Then, some techniques of improving RF WPT efficiency were investigated. It is reported that high-efficiency RF WPT can be achieved by using a directional narrow radiation beam of the antenna that can focus wireless power on the receiver.(4)

With a narrower antenna beam, the gain and directivity characteristics of the antenna increase. In practice, if the radiated power can be accurately and directly injected into the receiver antenna, more radiated transmission power will be obtained by the receiver and the WPT efficiency will be improved. However, a narrower antenna beam results in a smaller area for radiation reception. Because the radiation beam cannot be directly observed visually, it is difficult for the far-end receiver to accurately confirm the spatial location of the air radiation beam in order to obtain the highest transmission efficiency.

To realize techniques of visually confirming the spatial location of the radiation beam and of efficiently analyzing the spatial distribution of the beam power, a novel simple antenna beam sensor is designed and implemented in this study. The antenna beam sensor can support the far-end RF power receiver to easily and quickly find the location of the maximum air radiation power, whereby power will be transferred by the RF WPT system with high efficiency. Additionally, the sensor can measure the radiated power distribution in space, which will be helpful in studies of the energy loss during radiative transfer and useful for the development of microwave wireless transmission and microwave energy harvesting systems. In the following sections, the operation mechanism and design methods of the antenna beam sensor are introduced.

2. Antenna Beam Sensor

Many novel RF WPT system architectures have been published, and the main architecture of a typical RF WPT system is shown in Fig. 1.(5–7) The overall system includes an RF power transmitter, a radiation transmission path, and an RF power receiver. The RF power transmitter provides the RF power source and transmits the radiation power to air via the antenna. The receiver includes an RF rectenna and a power management module. The RF rectenna is

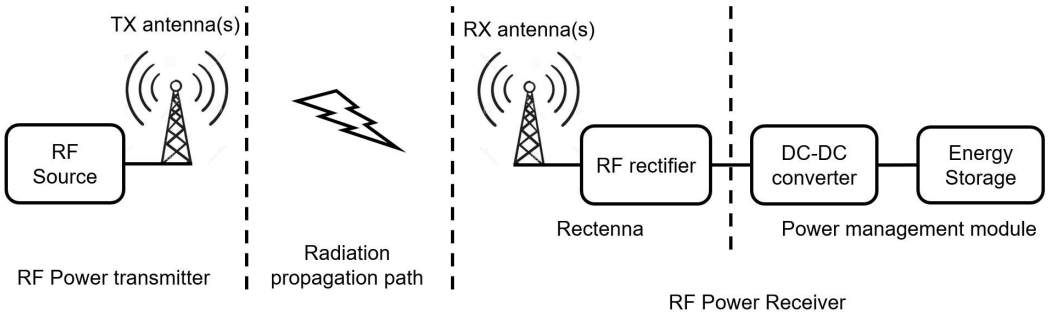

Fig. 1. Main architecture of a general RF WPT system.

integrated with an antenna and an RF rectifier.[8] The receiver antenna picks up the air radiation power and converts it to RF power. The RF rectifier converts the RF power into direct current (DC) power, and then the power management module stores the DC power into the energy storage. In this study, to detect the location of the air radiation beam easily and quickly, we designed a novel RF rectenna. The main structure of the proposed RF rectenna is shown in Fig. 2, and it is combined with a patch antenna, an RF rectifier, and a LED. The brightness of the LED of the RF rectenna will vary with the intensity of the received radiation power, and we can quickly determine the intensity of the received RF power by observing the light level of the LED. To make the rectenna more practical, we have designed a special RF rectifier to enable the LED to be lit even when the received power is weak. Furthermore, we arranged the 36 proposed rectennas into a 6 × 6 array to form the antenna beam sensor, as shown in Fig. 3, and we observed the spatial radiation power beam distribution as the brightness distribution of the LED array. The rectenna's antenna and RF rectifier design, and their integration into an antenna beam sensor are described in detail below.

2.1 Patch antenna design

A patch antenna is widely used in WPT systems because of its high gain and directivity in an orthogonal plane of the radiation source, as well as its simplicity and low cost.[4,7,9] Figure 4 shows that the patch antenna structure is formed by a dielectric substrate sandwiched between two metal layers. The bottom metal layer is used as the grounding metal, and the top metal layer is used as the radiating patch metal.

On the basis of the transmission line and cavity models,[10,11] a patch antenna is designed in transverse magnetic (TM) modes with the TM_{10} mode and patch length (L) and width (W) of the patch metal. The length and width are expressed by Eqs. (1) and (2), respectively, where c is the speed of light and ε_e is the effective dielectric constant given by Eq. (3), and f_r is the antenna operating frequency, which is 2.4 GHz in this study. The location of the feed point d can be determined using Eq. (4), where α is usually between 100 and 300 Ω, and $b = W / 2$ in this study.

$$L = \frac{c}{2f_r\sqrt{\varepsilon_e}} - 0.824h\frac{\left(\varepsilon_e + 0.3\right)\left(W/h + 0.264\right)}{\left(\varepsilon_e - 0.258\right)\left(W/h + 0.8\right)} \tag{1}$$

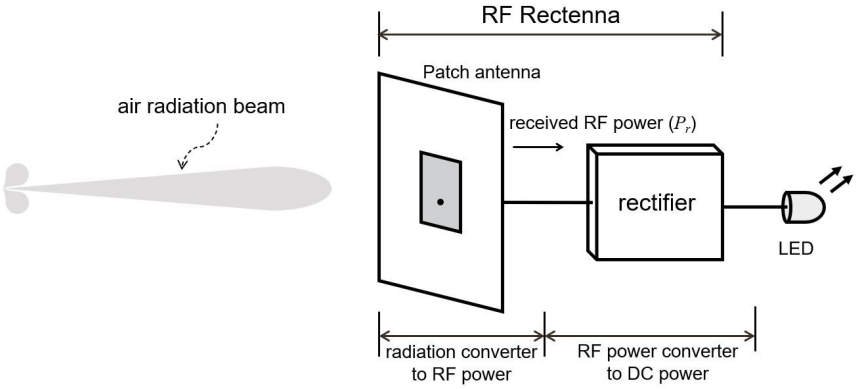

Fig. 2. Proposed novel RF rectenna, which is combined with a patch antenna, an RF rectifier, and a connected LED.

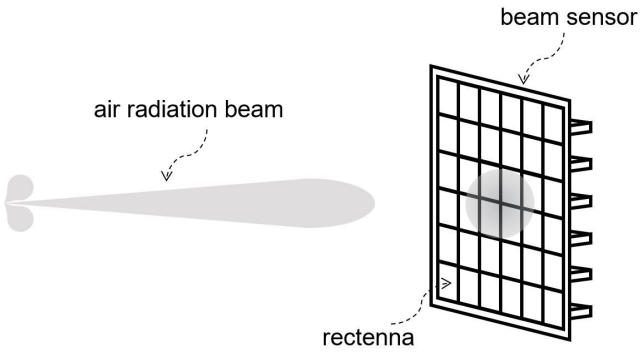

Fig. 3. Arrangement of 36 of the proposed rectennas to form the beam sensor.

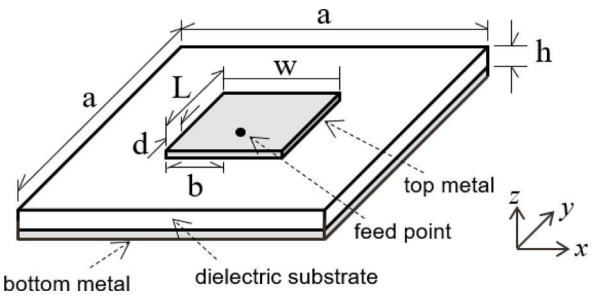

Fig. 4. Structure of a patch antenna.

$$W = \frac{c}{2f_r}\sqrt{\frac{2}{\varepsilon_r + 1}} \tag{2}$$

$$\varepsilon_e = \frac{\varepsilon_r + 1}{2} + \frac{\varepsilon_r - 1}{2}\left[1 + \frac{12h}{W}\right]^{-1/2} \tag{3}$$

$$d = \frac{\mathrm{L}}{\pi}\cos^{-1}\left(\sqrt{\frac{50}{\alpha}}\right) \tag{4}$$

In this study, the antenna was fabricated on an FR4 printed circuit board (PCB) substrate with a dielectric constant of 4.4 and a loss tangent of 0.02. We used the electromagnetic (EM) field computer-aided design tool (CST)[12] to establish a 3D patch antenna model for simulating electrical performance. The preliminary antenna size was estimated using Eqs. (1)–(4), and then the characteristics were optimized subsequently. The final dimensions of the antenna are listed in Table 1. Figure 5 shows the simulated reflection coefficient of the antenna; it attains 27 dB at the operation frequency of 2.4 GHz. The simulated 2.4 GHz radiation patterns are shown by dash lines in Fig. 6. Figure 6(a) shows a radiation graph in the *xz*-plane and Fig. 6(b) shows a radiation graph in the *yz*-plane. The simulated maximum gain is 6.4 dBi.

2.2 RF rectifier design

The RF rectifier is one of the most important circuits in the WPT system, and it converts the RF signal received through the antenna into a suitable DC supply voltage. In the past, many rectifier circuits have been reported. The earliest proposed rectifier circuit is the Villard circuit[13] consisting simply of a capacitor and a diode. It has the great benefit of simplicity, but its output has poor ripple characteristics. The Greinacher voltage doubler,[14] also called the Villard voltage doubler, is a significant improvement over the Villard circuit and its output ripple is much reduced. The most widely used rectifier circuit for WPT systems is the

Table 1
Size parameters of the patch antenna.

Dimension	*a*	*b*	*C*	*h*	*L*	*W*
Value (mm)	70	14.75	11.05	0.8	29.5	29.5

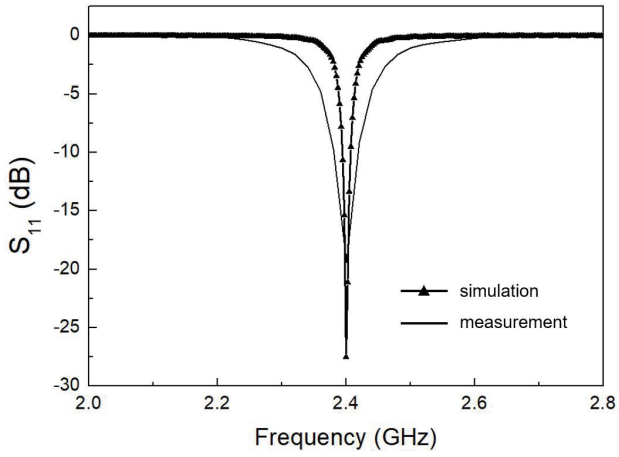

Fig. 5. Reflection coefficient characteristic of a patch antenna.

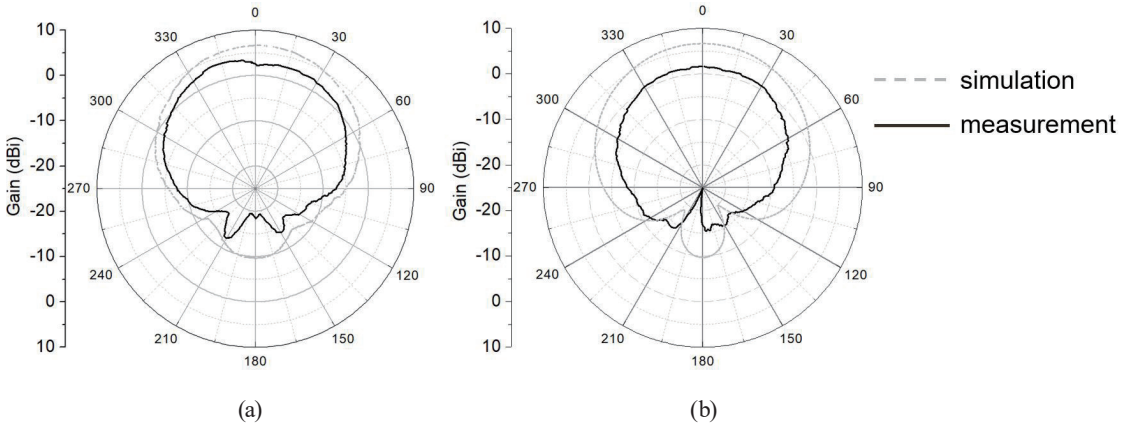

Fig. 6. Radiation patterns of the patch antenna at 2.4 GHz on (a) *xz*- and (b) *yz*-planes.

Cockcroft–Walton multiplier,[15,16] also known as the Greinacher multiplier. The multiplier circuit comprises many units of the Greinacher voltage doubler stacked in series, which converts RF power from a low voltage level to a higher DC voltage level. In this work, to improve the sensitivity of the antenna beam sensor, the Cockcroft–Walton multiplier is used in the RF rectifier to boost the output DC voltage to light the LED under weak received power.

Figure 7 shows an N-stage Cockcroft–Walton voltage multiplier circuit, and the subcircuit within the dash-line rectangle is a single stage, that is, a Greinacher voltage doubler. The function of a matching network at the input of the circuit is to lower impedance mismatch loss. To achieve a high output DC voltage and a high voltage conversion efficiency under weak received power, a ten-stage Cockcroft–Walton voltage multiplier is used as the RF rectifier in the antenna beam sensor. The output voltage V_{dc} of the multiplier circuit could be calculated as

$$V_{dc} = \left(2 \times N \times V_{max}\right) - \Delta V - \delta V, \tag{5}$$

$$\Delta V = \frac{1}{f \times C}\left(\frac{2 \times N^3}{3} + \frac{N^2}{2} - \frac{N}{6}\right), \tag{6}$$

$$\delta V = \frac{1 \times N \times \left(N+1\right)}{4 \times f \times C}, \tag{7}$$

where N is the number of stages, V_{max} is the peak input voltage, ΔV is the resultant voltage across the capacitors, and δV is the output ripple voltage (peak to peak). When the output load is connected, the resultant voltage will drop across capacitors, inducing effective current generation and output ripple voltage. The voltage load fluctuation is given by Eq. (6), where f is the signal frequency and C is the capacitance. The ripple voltage δV can be evaluated using Eq. (7). Equation (5) shows that the output voltage can be boosted by increasing the number of cascaded stages, but it will be limited by N times the breakdown voltage of the diode.

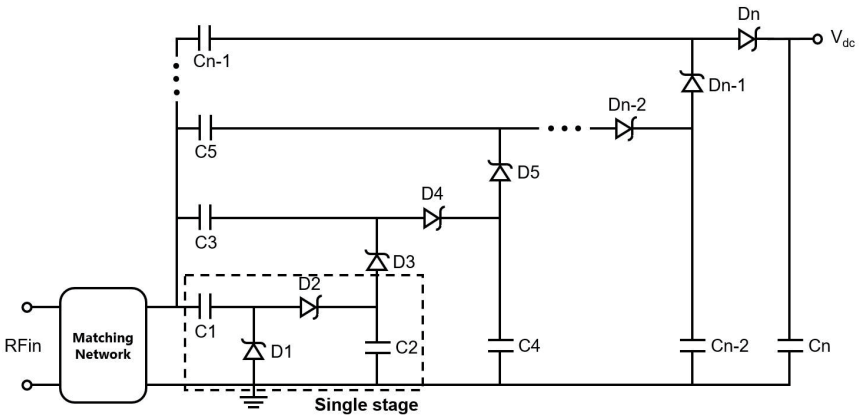

Fig. 7. N-stage rectifier circuit.

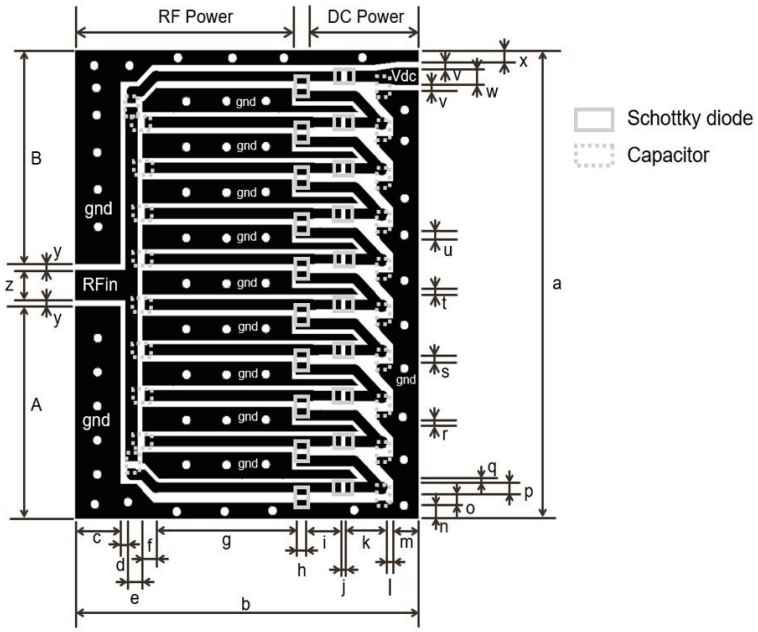

Fig. 8. Layout of the proposed ten-stage RF rectifier circuit.

We use the RF circuit simulator to design and simulate the performance of the RF rectifier. Figure 8 shows the layout of the proposed ten-stage RF rectifier circuit. The substrate of the circuit is a 0.8-mm-thick PCB with a dielectric constant of 4.4 and a loss tangent of 0.02. Solid-line rectangles indicate the locations of SMS7630 Schottky diodes[17] that act to decrease the device loss because of their low junction voltage. The main parameters of the Schottky diodes are listed in Table 2. Dash-line rectangles show the locations of the capacitors, which are 1-μF-capacitance muRata chip capacitors.[18] White circles mark the locations of via holes.

The EM simulator is used to evaluate the RF trace characteristics and parasitic effects of the layout. The EM simulation is combined with the models of the Schottky diodes and chip capacitors to cosimulate the overall performance of the ten-stage RF rectifier. As shown in

Table 2
Parameters of SMS7630 Schottky diodes.

Parameter	Value
Breakdown voltage B_v (V)	2
Built-in voltage V_{bi} (V)	0.34
Series resistance R_q (Ω)	20
Forward saturation current I_s (μA)	5
Junction capacity C_{jo} (pF)	0.14
Breakdown current I_{BV} (mA)	0.1
Ideal coefficient N	1.05

Table 3
Size parameters of the ten-stage RF rectifier in Fig. 8.

Dimension	*a*	*b*	*c*	*d*	*e*	*f*	*g*	*h*
size (mm)	47.2	34.9	4.8	0.61	1.2	1.8	15.36	1.05
Dimension	*i*	*j*	*k*	*l*	*m*	*n*	*o*	*p*
size (mm)	1.34	0.86	4.3	0.85	2.7	1.5	1	0.9
Dimension	*q*	*r*	*s*	*t*	*u*	*v*	*w*	*x*
size (mm)	0.38	0.38	0.98	0.6	1	0.62	1.7	1.1
Dimension	*y*	*z*	*A*	*B*				
size (mm)	0.64	3	21.4	21.5				

Fig. 8, the layout can be divided into two parts: the RF trace and the DC trace. The RF trace is where the RF signal travels before the diode rectifier, and the DC signal travels along the DC trace. We carefully design the width and length of ten RF traces to match the input impedance to 50 Ω. The size parameters of the layout after performance optimization are listed in Table 3.

The solid lines with triangles shown in Fig. 9 are the simulated results of the RF rectifier. Figure 9(a) shows the reflection coefficient frequency response. S_{11} is lower than −10 dB at the operation frequency of 2.4 GHz. Figure 9(b) shows the corresponding output voltage under various input powers when the output was connected to a 21 kΩ load.

3. Measured Results

In this section, we first introduce the measured results of the patch antenna and the RF rectifier. Then, we integrate them into the RF rectenna and arrange 36 RF rectennas into a 6 × 6 array to form the antenna beam sensor, and measure its functions and performance.

3.1 Measurement results for patch antenna

Figure 10(a) shows the photograph of the proposed patch antenna. We utilized the Anritsu MS46122B vector network analyzer (VNA) to measure the reflection coefficient of the antenna for comparison with simulated results, as shown in Fig. 5, where the solid line shows the measured reflection coefficient S_{11}, which is −19.4 dB at 2.4 GHz. Figure 5 shows that the simulated results agree with the measured results. The radiation pattern of the patch antenna was

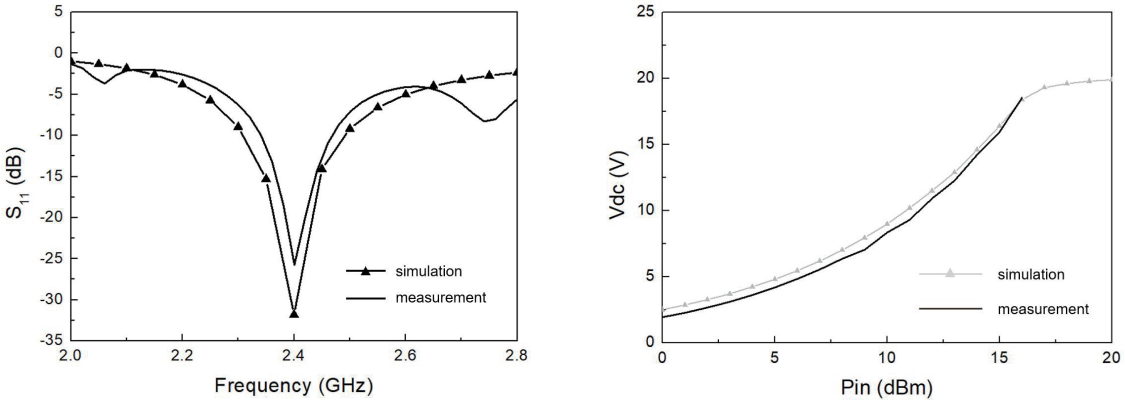

(a) (b)

Fig. 9. (a) Simulated and measured reflection coefficient characteristics of the RF rectifier. (b) Simulated and measured output voltage curves with various input powers.

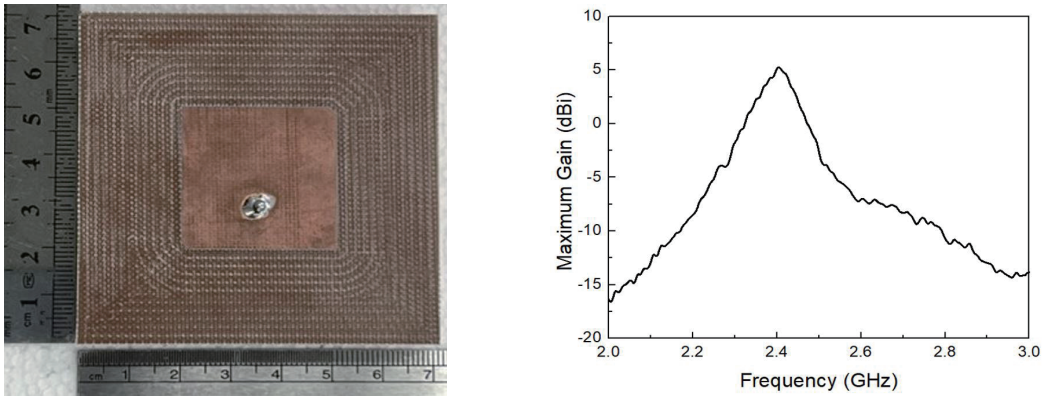

(a) (b)

Fig. 10. (Color online) (a) Photograph of the proposed patch antenna. (b) Measured maximum gain characteristic with various frequencies.

measured with the Atenlab A3 Over-the-Air (OTA) antenna measurement system[19] and the results are shown as solid lines in Fig. 6. The trend of the measured results is close to that of the simulated results. Figure 10(b) shows that the measured maximum gain is 5.2 dBi at 2.4 GHz.

3.2 Measurement results for RF rectifier

Figure 11 shows a photograph of the proposed RF rectifier. The VNA is utilized to measure the reflection coefficient of the rectifier, which is shown by the solid line in Fig. 9(a). The simulated result is close to the measured result. The measured S_{11} is −25 dB at 2.4 GHz. Additionally, we use the RF signal generator E4438C to generate a 2.4 GHz RF signal with a power intensity ranging from 0 to 16 dBm to feed into the RF rectifier and measure the output voltage when the output of the RF rectifier carries a 21 kΩ load. The measured voltage with

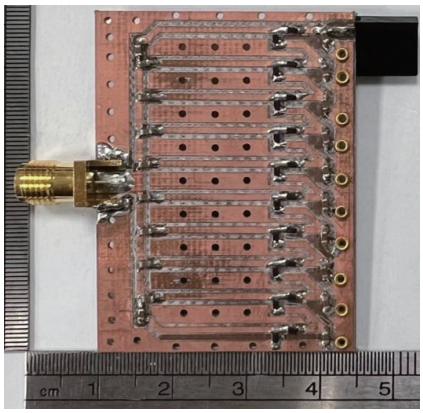

Fig. 11. (Color online) Photograph of the proposed RF rectifier.

(a) (b)

Fig. 12. (Color online) Photographs of the proposed antenna beam sensor. (a) Top and (b) side views showing the sensor weight of 1.15 kg.

various input powers is shown in Fig. 9(b), and the measured result agrees with the simulated result. The highest conversion efficiency, which is calculated as P_{DC}/P_{RF}, where P_{RF} is the input RF power and P_{DC} is the output DC power, attains a value of 50.38%.

3.3 Antenna beam sensor measurement

Figure 12 shows the photograph of the proposed antenna beam sensor. Because of its light weight of 1.15 kg, the sensor can be easily handled and moved for measurement work. An RF power transmitter with a high-directivity horn antenna, shown in Fig. 13(a), is utilized to generate a radiation beam. The maximum gain of the horn antenna is 14.9 dBi and the power transmitter can provide an output power of 38 dBm. When the RF power transmitter is turned on, a radiation beam is emitted by the antenna. The antenna beam sensor placed 5 m from the transmitter receives the radiation beam and converts it into power to light up the LED array, as

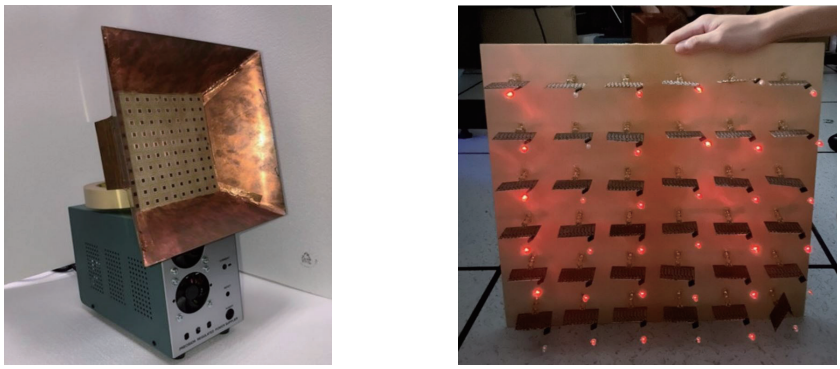

(a) (b)

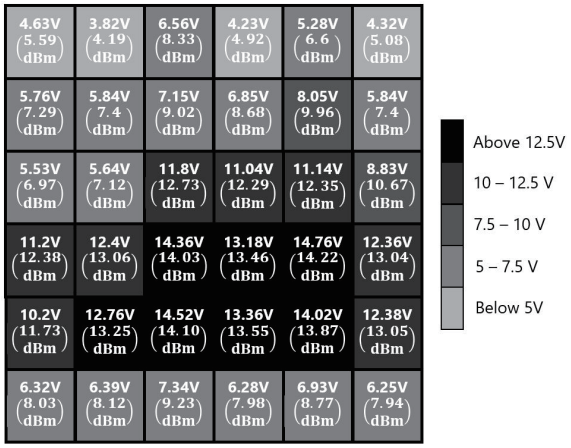

(c)

Fig. 13. (Color online) (a) Photograph of a 2.4 GHz power transmitter with a high-directivity horn antenna. (b) LED array lit by received power. (c) Position distribution of output voltage and corresponding received power.

shown in Fig. 13(b). The LED brightness distribution varies in accordance with the received RF power intensity distribution. We simultaneously measure the output voltage of each RF rectifier in the sensor, as shown in Fig. 13(c) for the corresponding position.

We can also estimate the received RF power (P_r) at each patch antenna using the relationship between the input power and the output voltage shown in Fig. 9(b). We invert the input power and output voltage in Fig. 9(b), and the input power of the RF rectifier here is the RF power received by the patch antenna. We can plot the curve of the received RF power with various output voltages, as shown in Fig. 14. In Fig. 14, the dash line is a curve of the received RF power fitted with a second-order polynomial expressed as

$$P_r = 0.11{V_{dc}}^2 + 0.39V_{dc} - 0.452. \tag{8}$$

During the detection of the radiation beam, we measured and recorded the output voltage of each RF rectifier in the sensor and showed the output voltage for the corresponding position in

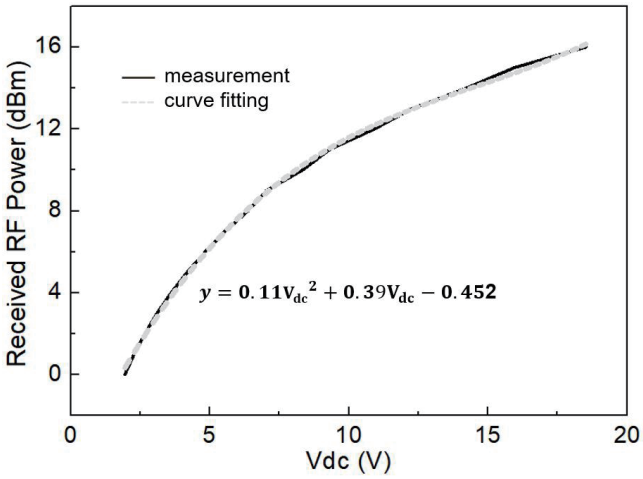

Fig. 14. Received RF power and its fitting curve with various output voltages.

Fig. 13(c). By utilizing Eq. (8), the received RF power was calculated and is given below the output voltage. The background color of the figure is adjusted with the output voltage level, and the spatial beam power intensity distribution can be clearly observed. As shown in Fig. 13(c), the darker location in the middle of the graph indicates the higher beam power intensity.

As mentioned above, we can utilize the sensor to quickly identify the location of the maximum beam power on the basis of the LED brightness and to infer the received power intensity distribution from the output voltage level distribution. The proposed antenna beam sensor will be useful in the research on wireless power transfer, microwave energy harvesting, and radiation beam behavior in air.

4. Conclusions

A novel portable 2.4 GHz antenna beam sensor was implemented in this study. The antenna beam sensor was assembled as a 6 x 6 RF rectenna array, and each RF rectenna output was visualized as an illuminated LED. By utilizing the proposed sensor, the spatial radiation beam distribution was quickly observed visually, and the spatial radiation power distribution was also measured. The RF rectenna of the sensor was integrated with a patch antenna with a measured gain of 5.1 dBi and a high-efficiency RF–DC conversion circuit with a measured conversion efficiency of 50.38%. Under microwave WPT system operation, the sensor enabled us to observe the change in the distribution of the radiation beam power in the space transmission channel and obtain information related to the maximum energy transmission efficiency in a convenient manner. The overall size of the antenna beam sensor was 42 × 42 cm^2 and its weight was 1.15 kg. Therefore, the sensor is light and easy to handle, which makes it easy to carry for measurement work. The proposed antenna beam sensor is a useful tool for use in the development of the WPT and energy harvesting systems.

References

1 Transforma Insights: https://transformainsights.com/news/iot-market-24-billion-usd15-trillion-revenue-2030 (accessed June 2022).
2 S. Y. R. Hui, W. Zhong, and C. K. Lee: IEEE Trans. Power Electron. **29** (2014) 9. https://doi.org/10.1109/TPEL.2013.2249670
3 B. Clerckx, R. Zhang, R. Schober, D. W. K. Ng, D. I. Kim, and H. V. Poor: IEEE J. Sel. Areas Commun. **37** (2019) 1. https://doi.org/10.1109/JSAC.2018.2872615
4 Q. Hui, K. Jin, and X. Zhu: IEEE Trans. Ind. Electron. **67** (2020) 8. https://doi.org/10.1109/TIE.2019.2941150
5 H. Huang and T. Li: IEEE Antennas Wirel. Propag. Lett. **15** (2016) 1495. https://doi.org/10.1109/LAWP.2016.2514534
6 M. AbdelHafeez, K. Yousef, M. AbdelRaheem, and E. E. M. Khaled: 2019 Int. Conf. Innovative Trends in Computer Engineering (2019) 365. https://doi.org/10.1109/ITCE.2019.8646558
7 J. H. Park, D. I. Kim, and K. W. Choi: IEEE Access **9** (2021) 2018. https://doi.org/10.1109/ACCESS.2020.3047485
8 S. Shen, C. Chiu, and R. D. Murch: IEEE Trans. Antennas Propag. **66** (2018) 2. https://doi.org/10.1109/TAP.2017.2786320
9 S. A. Rotenberg, S. K. Podilchak, P. D. H. Re, C. Mateo-Segura, G. Goussetis, and J. Lee: IEEE Trans. Microwave Theory Tech. **68** (2020) 5. https://doi.org/10.1109/TMTT.2020.2968055
10 K. Carver and J. Mink: IEEE Trans. Antennas Propag. **29** (1981) 1. https://doi.org/10.1109/TAP.1981.1142523
11 J.-H. Kim, H.-Y. Yu, and C. Cha: 2014 IEEE Wireless Power Transfer Conf. (2014) 2881. https://doi.org/10.1109/WPT.2014.6839565
12 CST Studio Suite: https://www.3ds.com/products-services/simulia/products/cst-studio-suite/?utm_source=cst.com&utm_medium=301&utm_campaign=cst (accessed June 2022).
13 E. Everhart and P. Lorrain: Rev. Sci. Instrum. **24** (1953) 221. https://doi.org/10.1063/1.1770669
14 S. Patel and D. B. Dave: Int. J. Eng. Trends and Technol. **4** (2013) 4. http://www.ijettjournal.org/archive/ijett-v4i4p239
15 J. D. Cockcroft and E. T. S. Walton: Proc. Royal Society A **136** (1932) 619. http://doi.org/10.1098/rspa.1932.0107
16 J. D. Cockcroft and E. T. S. Walton: Proc. Royal Society A. **137** (1932) 229. https://doi.org/10.1098/rspa.1932.0133
17 SMS7630 Schottky diodes data sheet: https://www.skyworksinc.com/-/media/SkyWorks/Documents/Products/201-300/Surface_Mount_Schottky_Diodes_200041AG.pdf. (accessed June 2022).
18 muRata chip capacitor: https://www.murata.com/en-us/products/capacitor/ceramiccapacitor/overview/lineup#smd (accessed June 2022).
19 Atenlab A3 Over-the-Air (OTA) antenna measurement system: https://en.atenlab.com.tw/book-1.html (accessed June 2022).

About the Authors

Ja-Hao Chen received his B.S. degree in electronics engineering from Fu-Jen University, Taipei, Taiwan, in 1997 and his Ph.D. degree in electrical engineering from the National Cheng Kung University, Tainan, Taiwan, in 2002. From 2002 to 2005, he was with ALi Corporation, Taipei, Taiwan, where he worked on on-chip analog and digital I/O pads and ESD protection circuit design. From 2005 to 2007, he was with RichWave, Taipei, Taiwan, where he worked on on-chip RF power amplifier and RF switch circuit design. From 2007 to 2012, he was with the Department of Electrical Engineering, Tunghai University, Taichung, Taiwan, as an assistant professor. He is currently an associate professor in the Department of Communication Engineering, Feng-Chia University, Taichung, Taiwan. His research interests include on-chip RF circuit design and antennas for sensor and wireless power transfer applications. (chiahaoc@fcu.edu.tw)

Yu-Chang Lin received his B.S. degree in electronics engineering from Chien-Kuo Technology University, Chang-Hua, Taiwan, in 2002. From 2003 to 2005, he was with AlfaPlus Semiconductor Inc., Hsin-Chu, Taiwan, where he worked on on-chip RF power amplifier circuit design. From 2005 to 2009, he was with Merry Electronics Co., Ltd., Taichang, Taiwan, where he worked on bluetooth headset circuit design. From 2010 to 2015, he was with apm Communication, Inc., Hsin-Chu, Taiwan, where he worked on designing wifi and bluetooth combo modules for System-in-Package. He is currently pursuing a Ph.D. degree under the Ph.D program of electrical and communications engineering of Feng-Chia University, Taichung, Taiwan. His research interests include RF system circuit design and wireless power transfer applications. (a7ptaco@seed.net.tw)

Tai-Chieh Tseng received his B.S. degree in communication engineering from Feng-Chia University, Taichung, Taiwan, in 2020. He is currently pursuing an M.S. degree in communication engineering from Feng-Chia University, Taichung, Taiwan. His research interests include on-chip RF circuit design and antennas for sensor and wireless power transfer applications. (gary2008tsengtw@gmail.com)

Cheng-Chi Yu received his B.S. degree in electrical engineering from Feng-Chia University, Taichung, Taiwan, in 1985, and his M.S. and Ph.D. degrees in electrical engineering from National Cheng Kung University, Tainan, Taiwan, in 1991 and 1995, respectively. From 1995 to 2005, he worked as an associate professor in the Department of Electrical Engineering, Nan-Kai University of Technology, Nantou, Taiwan. In 2005, he joined the Department of Communications Engineering, Feng-Chia University, Taichung, Taiwan, where he is currently an associate professor. His research interests include antennas, microwave components, and radio-frequency integrated circuits (RFICs). (ccyu@fcu.edu.tw)